Wasserstein Distance-based Expansion of Low-Density Latent Regions for Unknown Class Detection

Prakash Mallick, Feras Dayoub. Jamie Sherrah
Australian Institute of Machine Learning
North Terrace, Adelaide SA 5000
{prakash.mallick, feras.dayoub, jamie.sherrah}@adelaide.edu.au

Abstract

This paper addresses the significant challenge in open-set object detection (OSOD): the tendency of state-of-the-art detectors to erroneously classify unknown objects as known categories with high confidence. We present a novel approach that effectively identifies unknown objects by distinguishing between high and low-density regions in latent space. Our method builds upon the Open-Det (OD) framework, introducing two new elements to the loss function. These elements enhance the known embedding space's clustering and expand the unknown space's low-density regions. The first addition is the Class Wasserstein Anchor (CWA), a new function that refines the classification boundaries. The second is a spectral normalisation step, improving the robustness of the model. Together, these augmentations to the existing Contrastive Feature Learner (CFL) and Unknown Probability Learner (UPL) loss functions significantly improve OSOD performance. Our proposed OpenDet-CWA (OD-CWA) method demonstrates: a) a reduction in open-set errors by approximately $17\% - 22\%$*, b) an enhancement in novelty detection capability by* $1.5\% - 16\%$*, and c) a decrease in the wilderness index by* $2\% - 20\%$ *across various open-set scenarios.*

1. Introduction

Object detectors typically operate under a closed-set assumption, expecting that testing scenarios will only involve object categories from the training datasets. However, in real-world applications, these systems often encounter unseen object categories, leading to significant performance degradation. This limitation becomes evident in scenarios where detectors misclassify unfamiliar objects with high confidence [29]. Addressing this, Open-set Object Detection (OSOD) [12, 14, 24] has emerged, focusing on detecting both known and unknown objects in diverse conditions.

In this paper, our emphasis is on an approach guided by the widely recognised principle that familiar objects tend to aggregate, creating high-density regions within the latent space. Conversely, unknown objects or novel patterns are commonly dispersed in low-density regions [5, 11]. Notably, Han *et al*. [12] successfully identified unknowns without relying on complex pre-processing procedures in their work. Although this type of OSOD has improved the practicality of object detection by enabling detection of instances of unknown classes, there is still substantial room for improvement; e.g., one can refer to Fig. 1, that shows detector trained using [12] suffers from misclassifications. These open-set errors are as a result of compactness in clusters that can be further enhanced using combination of ideas from Miller *et al*. [25] and Courty *et al*. [6]. Additionally, motivated from Liu *et al*. [19], we leverage the distance awareness property of the model to properly quantify the distance of a testing example from the training data manifold through

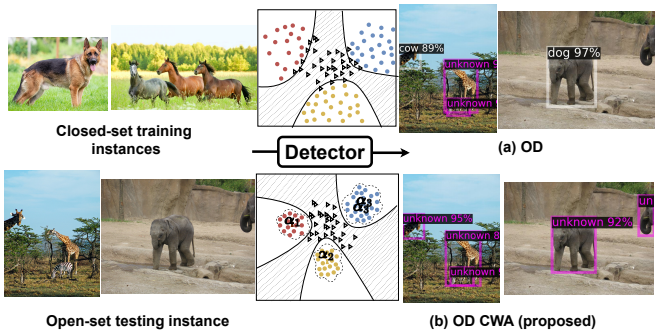

Figure 1. Model trained on an existing method, i.e., Open-Det (OD) (both ResNet and Transformer-based) is proficient at identifying unknown entities to a certain extent but remains largely susceptible to misclassification of a diverse range of unfamiliar elements (black triangles, e.g. zebra, elephant) into known classes (coloured dots, e.g. dog, cow). (b) Our method identifies unknown objects by enhancing the compactness among proposal features, thereby assisting the uncertainty-based optimiser in extending low-density regions (dotted striped regions in between boundaries) beyond the baseline (OD).

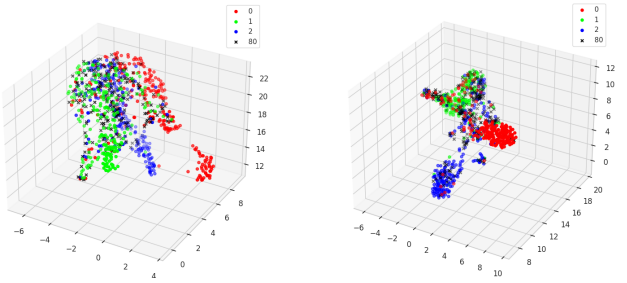

(a) OD (b) OD-CWA

Figure 2. U-MAP [23] visualisation of latent features. Three VOC classes (coloured dots; id - $0, 1, 2$) are known classes, and non-VOC classes (black cross; id - 80) in COCO as unknown classes. OD-CWA exhibits better separation as compared to OD in-terms of both open-set and closed-set classes.

spectral normalisation of the weights.

In brief, the features for known classes are extracted and compactness of those features are enhanced, which in turn dictates more low-density regions for unknown classes. Then, an unknown probability as per Han *et al*. [12] is determined for each instance that serves as a threshold mechanism to distinguish low-density regions surrounding the clusters of known classes. One can visualise the latent features[1] for three VOC classes (coloured dots), which are known classes, and non-VOC classes (black cross) in MS-COCO that are unknown classes; see e.g., Fig. 2.

The contributions of this research can be summarised as follows, with references to relevant works:

- We develop a new approach, called OD-CWA, based on the Wasserstein distance (optimal transport [6, 31]) within the framework of metric learning. To the best of our knowledge, Wasserstein distance is utilised here for the first time to demonstrate OSOD. As a result of this novel setting, we demonstrate its capability in yielding promising outcomes, fostering an enhanced distinguish-ability between the known and unknown classes including flagging of unknown classes.
- We leverage the concept of spectral normalisation into the output linear layer that leads to the improvement of the overall effectiveness of the approaches.
- The approach OD-CWA when compared to previous methods, exhibits significant improvements on four open-set metrics when evaluated on three different datasets, e.g., OD-CWA reduces absolute open-set errors by $17\% - 22\%$ and increases the novelty detection ability by $1.5\% - 16\%$. Moreover, the incorporation of these new loss functions leads to enhanced intra-class and inter-class clustering compared to the baseline OD, facilitating the expansion of low-density latent regions.

[1]Please note that we only show a small subset of classes as it provides a better visualisation of known.

The paper is organised as follows: Section 2 delves into open-set object detection, providing an overview of the existing work, background information, and the motivation driving the development of open-set detectors. The subsequent section 3 describes the underlying problem. Following which, Section 4 provides understanding of a peculiar mathematical concept, how and where we fit it in this framework of open-set detection. Next, section 5 throws light on the setup and brief description of this novel approach. Following which, Section 6 carries out an extensive experimental evaluation of this approach on detection metrics. Then, Section 7 will summarise the research, highlighting certain limitations, and suggesting potential avenues for future work.

2. Background and Related Work

Open-set Object Detection: Initial endeavours by Scheirer *et al*. [29] pioneered the investigation of open-set recognition, addressing incomplete knowledge during training where previously unseen classes may arise during testing. They devised a one-vs-rest classifier to identify and reject samples from unknown classes. Subsequently, Scheirer*et al*. [30], have expanded upon their foundational framework to further enhance the capabilities and performance of open-set recognition. Further, research by [24, 25] has provided great insights into the utilisation of label uncertainty in open-set object detection using dropout sampling (DS) and leveraging the power of Gaussian mixture models (GMM) to capture likelihoods for rejecting open-set error rates, which are required for safety-critical applications. The complex post-processing steps involved with fitting GMMs, coupled with the reduced dispersion of low-density latent regions, lead to confident open-set errors that impede its usage in practical applications. An additional array of prevalent techniques for extracting epistemic uncertainty hinge on resource-intensive sampling-based methodologies, such as Monte Carlo (MC) Dropout [10] and Deep Ensembles [16]. These approaches, although holding promise in the realm of OSOD [16, 24], carry a notable computational burden as they necessitate multiple inference passes for each image.

Open World Object Detection and Grounding DINO

In the context of object detection, "Open World Object Detection" (ORE) has gained prominence [14]. This paradigm requires models to perform two crucial tasks: identifying previously unknown objects without prior supervision and continually learning these new categories without forgetting previously learned ones. To address these two tasks, ORE utilises contrastive clustering and energy-based methods to identify and integrate unknown objects. Similar, albeit with a slightly different purpose, a recent methodology called Grounding DINO [20] has been introduced. This method involves the integration of the

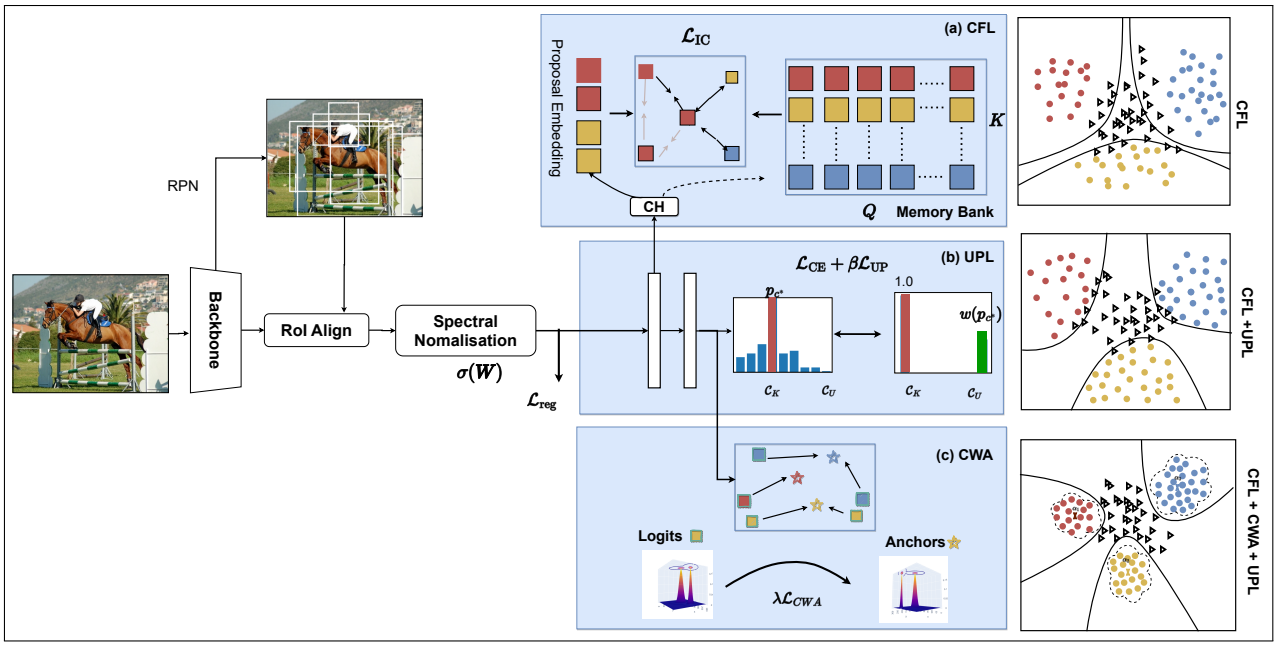

Figure 3. OD-CWA consists of a Contrastive Feature Learner (CFL), Spectral Normalisation (SN), Class Wasserstein Anchor Learner (CWA) and Unknown Probability Learner (UPL). The CFL [12] components utilises proposal features encoded into low-dimensional embeddings using the Contrastive Head (CH) optimised using Instance Contrastive Loss ($\mathcal{L}_{IC}$). The weights of the linear output layer are passed through a spectral normalisation step that maintain distance awareness property. Then UPL component utilises the cosine distances between embeddings and spectral normalised weights to learn the probabilities for both known classes (C_K) and the unknown class (C_U). The class Wasserstein anchor($\mathcal{L}_{CWA}$) part aids both CFL & UPL to increase the compactness in the clusters by finding the optimal transport plan from the logit space to anchor space. There is a visual illustration exhibiting the working of different components. Coloured dots and triangles represent reduced dimension of proposal features of different known and unknown classes, respectively. Coloured square represents proposal embeddings, and coloured + sketched squares inside CWA box represents scaled and transformed logits.

Transformer-based detector DINO [36] with grounded pre-training techniques, which empowers the detector to identify myriad objects based on category inputs by humans, allowing it to identify pre-defined object categories. In this approach, language is introduced as a means to imbue a traditionally closed-set detector with the capability for open-set concept generalisation. This particular concept is high on generalisation, moderate on adaptability (since it's not focused on learning over time but could be adapted to), and moderate on recognition scope since it deals with a broad range of categories but doesn't necessarily focus on detecting unknown unknowns. On the other hand, OSOD would be positioned with moderate generalisation, low adaptability, and broad recognition scope. We perceive the terms OSOD [12, 37], ORE [14], and open-vocabulary object detection (OVD) [35] as inherently distinct, despite some overlap. Collectively, they can be conceptualised to exist along a spectrum encompassing *recognition score, adaptability over time*, and *generalizability*, as illustrated in Fig. 4. Generalisation capability represents the model's ability to generalise beyond its training data, from specific known categories (low generalisation) to a

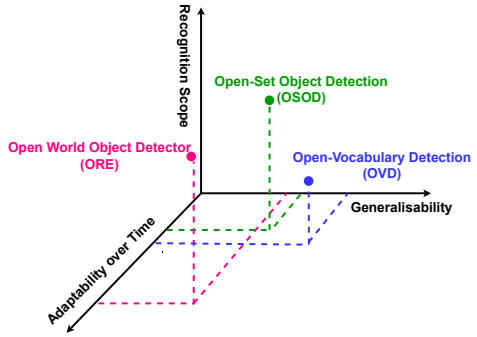

(a) OD

Figure 4. Comparing ORE, OSOD and OVD in terms of generalizability, adaptability over time and scope of recognition.

wide range of categories described in natural language (high generalisation). Adaptability over time denotes a model's ability to learn and incorporate new information over time, ranging from static models that do not learn from new data (low adaptability) to dynamic models that continuously update themselves with new categories (high adaptability). Recognition scope reflects the scope of recognition, from

recognising only known classes (narrow scope) to detecting and acknowledging the presence of completely unseen classes (broad scope). Our proposed method lies in the spectrum surrounding the point denoted by green colour.

3. Open-Set Detection Problem Statement

In an open-set detection task, one needs to detect the classes that are **seen/known** by the model (denoted as $C_{\mathcal{K}}$) and also flag the classes that are unseen by the model (denoted as $C_{\mathcal{U}}$). Let's denote the training samples $\mathcal{D}_{\text{closed}} := \{\mathbf{Z}_i = (\mathbf{x}_i, y_i)\}_{i=1}^{N_C}$, where i is an instance, and is drawn from a product space $\mathcal{Z}_k = \mathcal{X} \times \mathcal{Y}_k$, where $\mathcal{X}$ and $\mathcal{Y}_k$ are the input space and label space respectively. The following is the underlying problem which this paper is trying to solve/deliver:

- Detector to classify and detect correctly a closed set class i.e., to devise a classifier $h = g \circ f$, where h is the composition of functions (likely hidden residual blocks), where f is the output of the initial operation, that will lead to features and g processes that output further to deliver logits. This is done in a way that optimises the standard objective: $\frac{1}{N_C}\sum_{i=1}^{N_C}\left[y_i = \arg\max_{c \in \mathcal{Y}_C} f(\mathbf{x_i})_{y_i})\right]$, where N_C is the number of closed set samples and C refers to the total number of known classes.
- Detector to identify the open-set detections and flag them into a broader class of unknown using some form of score function.The score function can take various formulations, and we employ a specific unknown optimisation approach from the literature, detailed in subsequent sections.

4. OSOD as an optimal-transportation problem

Due to the prominence of Wasserstein distance in representational learning, domain adaptation [6, 31] and generative adversarial networks [2] we leverage this ideology and adapt it to the OSOD problem. Before diving into the details of how to pose Wasserstein distance inside OSOD, we first provide a detailed understanding of the Wasserstein metric.

Wasserstein Distance is a distance measure between probability distributions on a given metric space (M, ρ), where $\rho(x, y)$ is a distance function for two instances x and y. The p-th Wasserstein distance between two Borel probability measures[2] $\mathbf{P}$ and $\mathbf{Q}$ is defined as,

Definition 1 (Shen *et al.* [31]) *For $p \geq 1$, the p-Wasserstein distance between two distribution $\mathbf{P}$ and $\mathbf{Q}$ is given by,*

$$\mathcal{W}(\mathbf{P}, \mathbf{Q}) \triangleq \left[\inf_{\theta} \int_{X \times X} d(x, y)^p, d\theta(x, y)\right]^{\frac{1}{p}} \quad (1)$$

[2]The definition of measurable space can be found [4, Page 160]

The term $d(x, y)^p = ||x - y||^p$ represents the cost and $\mathbf{P}, \mathbf{Q} \in \{\mathcal{P} : \int d(x, y)^p \, d\mathbf{P}(x) < \infty, \forall y \in M$ are two probability measures with finite p-th moment. This metric fundamentally arises in the optimal transport problem, where $\theta(x, y)$ is a policy for transporting one unit quantity from location x to location y while satisfying the constraint $x \sim \mathbf{P}$ and $y \sim \mathbf{Q}$. When the cost of transporting a unit of material from $x \in \mathbf{P}$ to $y \in \mathbf{Q}$ is given by $d(x, y)^p$, then $\mathcal{W}(\mathbf{P}, \mathbf{Q})$ is the minimum-expected transport cost. Please note that solving $\mathcal{W}(\mathbf{P}, \mathbf{Q})$ is a challenge and therefore pioneering work according to the Kantorovich-Rubinstein theorem deals with the dual representation of the first Wasserstein distance that can be expressed as an integral probability metric [32]:

$$\mathcal{W}_1(\mathbf{P}, \mathbf{Q}) = \sup_{\|f\|_{\text{Lip}} \leq 1} \left(\mathbb{E}_{x \sim \mathbf{P}}[f(x)] - \mathbb{E}_{x \sim \mathbf{Q}}[f(x)]\right), \quad (2)$$

where the Lipschitz semi-norm is defined as $\|f\|_{\text{Lip}} = \sup |f(x) - f(y)| / d(x, y)$. In order to make a tractable computation of $\mathcal{W}_1(\mathbf{P}, \mathbf{Q})$, an algorithm[3] called as Sinkhorn-Knopp [1] algorithm is utilised. This is an iterative algorithm used to compute an approximate optimal transport plan $T_{k,l}$ for two probability distributions ($\mathbf{P}$ and $\mathbf{Q}$) while applying a regularisation as per the equation below,

$$D_{\text{SH}}(T; \mathbf{P}, \mathbf{Q}) = \sum_{k,l} T_{k,l} d_{k,l}(x, y) - \rho \cdot \sum_{k,l} T_{k,l} \log(T_{k,l})) \quad (3)$$

where ρ is smoothing parameter and k, l are elements (can be matrix variate) sampled from $\mathbf{P}$ and $\mathbf{Q}$.

Remark 4.1 *In the context of the paper, the distribution of $\mathbf{P}$ would refer to the distribution of anchors $\mathbf{A} \in \mathbb{R}^{B \times K \times K}$ and $\mathbf{Q} \in \mathbb{R}^{B \times K \times K}$ is the distribution of logits $\mathbf{L}$, where $B = 512 \times b$, where b is the batch size, and K is the total number of known classes. The class anchor clustering by [26] takes into account $||\mathbf{L} - \mathbf{A}||_2$. However, in a higher-dimensional space, namely $\mathbb{R}^{B \times K \times K}$, the estimation of parameters for deep neural networks that optimally transfer the samples of distributions of two probability spaces ($\mathbf{L}$ and $\mathbf{A}$) can be more effectively addressed through the lens of optimal transport, as encapsulated by the Wasserstein distance (2). This concept serves as the cornerstone of this paper.*

5. Methodology

We employ the Faster R-CNN [28] framework consisting of a backbone, Region Proposal Network (RPN), and region-convolutional neural network (R-CNN) that follows the architecture by Han *et al.* [12]. We augment the cosine

[3]Details can be found in Ramdas *et al.* [27].

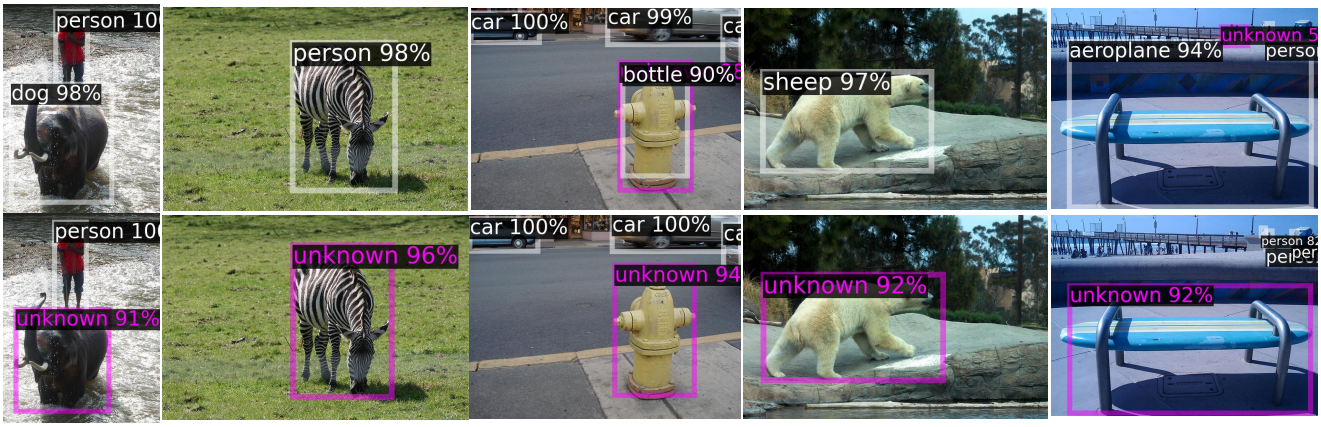

Figure 5. Qualitative comparisons between proposed OD (top) and OD-CWA (bottom). Both models are trained on VOC and the detection results are visualised using images from COCO. The purple colour represents unknown and white represents known. White annotations represent classes seen by the model and purple annotation correspond to unknown classes.

similarity-based classifier by introducing a spectral normalisation of the weights to the final linear layer. Some of the details are delineated below.

5.1. Spectral Normalisation of Weights to Linear Layer

This specific configuration draws inspiration from Liu et al. [19] which explains that deep learning models, e.g., ResNets, Transformers, often adopt residual architecture blocks, represented as $h(\mathbf{x}) = h_{L-1} \circ \ldots \circ h_2 \circ h_1(\mathbf{x})$, where $h_l(\mathbf{x}) = g \circ f$ refers to hidden units of layer l. They also mention that hidden mapping can be made to have meaningful relationship to the distance in input space. This is called distance preserving property that quantifies the distance from training data manifold and can be carried out by constraining Lipschitz constants of layers in the residual mappings g_l. We utilise this concept to ensure that the weight matrices linked with linear final residual block $g_1(\mathbf{x})$ has a spectral norm, i.e., the largest singular value as less than 1 and is due to the inequality $\|g_l\|_{\text{Lip}} \leq \|W_l\mathbf{x} + b_l\|_{\text{Lip}} \leq \|W_l\|_2 \leq 1$, where $l = 1$. Therefore, we employ spectral normalisation (SN) on the weight matrices, $\{W_l\}_{l=1}$ i.e., last layer. Subsequently, the spectral normalised weights are utilised in conjunction with the features within a scaled cosine similarity scoring function, producing output logits as follows: $\mathbf{L}_{i,j} = \frac{\alpha \cdot \mathbf{F}(\mathbf{x})_i^T \cdot \mathbf{w}_j}{\|\mathbf{F}(\mathbf{x})_i\| \cdot \|\mathbf{w}_j\|} \in \mathbb{R}^{m \times C}$, where $\mathbf{L}_{i,j}$ signifies the similarity score between the i-th proposal features $\mathbf{F}(\mathbf{x})_i$ and the weight vector $\mathbf{w}_j$ of class j, m denotes the multi-level features, and C is the total number of known classes. The scaling factor α is set to 20, and the box regressor is configured to be class-agnostic as per Han et al. [12].

5.2. Supervised Contrastive Loss

The primary purpose of this component of the loss is to create compactness between detections of individual classes (intra-class). This compactness and separation ultimately leads to expansion of low-density latent regions by narrowing the cluster of known classes. Motivated from Han *et al*. [12] i.e., CFL contains a contrastive head (CH), a memory bank and an instance level contrastive loss function $\mathcal{L}_{IC}$ and each proposal feature $\mathbf{F}(\mathbf{x})_i$ is encoded into an embedding with CH, that is optimised from the memory bank with the help of $\mathcal{L}_{IC}$. The formulation of $\mathcal{L}_{IC}$ is described by, $\mathcal{L}_{IC} = \frac{1}{N}\sum_{i=1}^{N}\mathcal{L}_{IC}(\mathbf{z}_i)$, where,

$$\mathcal{L}_{IC}(\mathbf{z}_i) = \frac{-1}{|M(c_i)|} \sum_{\mathbf{z}_j \in M(c_i)} \log \frac{\exp(\frac{\mathbf{z_i} \cdot \mathbf{z_j}}{\tau})}{\sum_{\mathbf{z}_k \in A(c_i)} \exp(\frac{\mathbf{z_i} \cdot \mathbf{z_k}}{\tau})},$$

and $\mathbf{z}_i$ corresponds to the embeddings of i^{th} proposal and τ is the temperature parameter. For detail about this loss function, one can follow Khosla *et al*. [15].

5.3. Class Wasserstein Anchor Loss

This approach is motivated from Miller *et al*. [26] and Wen *et al*. [33] that utilises the centre loss function as per,

$$\mathcal{L}_{CWA} = \sum_{i=1}^{m} \mathcal{W}(\mathbf{L}_i, \mathbf{A}_{y_i}), \tag{4}$$

where $\mathbf{A}_{y_i} \in$ is the class anchor centres of deep features corresponding to y^{th} class and $\mathbf{L}_i$ denotes the spectral normalised scaled logits as mentioned in Section 5.1. The function $\mathcal{W}$ is computed as per Eq. (1) and approximated as per Eq. (3) using iterative methods laid out in the implementation section.

5.4. Unknown Probability Loss

Unknown Probability Loss is an integral part of the primary loss function, which works in conjunction with CFL and CWA to enhance the scattering of the low-density regions around the cluster of known classes. The SN-transformed logits, $\mathbf{L}_i$ of a proposal are passed through a softmax function that leads to a softmax cross entropy (CE) loss $\mathcal{L}_{CE} = \sum_{c \in C} y_c \log(p_c)$, where $y_c = 1$ when $c = c^t$ is a ground truth class, $p_c = \frac{\exp(\mathbf{L}_c)}{\sum_{j \in C} \exp(\mathbf{L}_j)}$ and $C = C_{\mathcal{K} \cup \mathcal{U} \cup \text{bg}}$ that denotes all known, unknown inclusive of background. This CE loss along with a weighted formulation of entropy that acts as an uncertainty signal is utilised for constructing the unknown probability loss function $\mathcal{L}_{UP} \triangleq -w(p_{c^t}) \log(\bar{p}_{\mathcal{U}}))$, where $\bar{p}_{\mathcal{U}} \triangleq \frac{\exp(\mathbf{L}_c)}{\sum_{j \in C \setminus \{c^t\}} \exp(\mathbf{L}_j)}$ is the softmax without the logit of the ground truth class c^t. The term, $w(p_{c^t}) = (1 - p_{c^t})^{\alpha} p_{c^t}$. Further details about optimising this function can be found in Han *et al*. [12].

5.5. Optimisation Objective Function

The combined loss function employed in this paper can be trained in an end-to-end manner as follows:

$$\mathcal{L}_{\text{OD-CWA}} = \bar{\mathcal{L}} + \sigma\big[\lambda \mathcal{L}_{CWA} + \beta \mathcal{L}_{UP} + \mathcal{L}_{CE}\big] + \delta_k \mathcal{L}_{IC}, \tag{5}$$

$$\mathcal{L}_{\text{OD-SN}} = \bar{\mathcal{L}} + \sigma\big[\beta \mathcal{L}_{UP} + \mathcal{L}_{CE}\big] + \delta_k \mathcal{L}_{IC}, \tag{6}$$

where, $\bar{\mathcal{L}} = \mathcal{L}_{rpn} + \mathcal{L}_{reg}$, σ denotes SN component, $\mathcal{L}_{CWA} = \mathcal{W}_1(\mathbf{P}, \mathbf{Q})$, as per (2) and evaluated in an iterative manner based on eq (3) and $\mathcal{L}_{\text{rpn}}$ denotes the total loss of RPN, $\mathcal{L}_{\text{reg}}$ is the smooth L_1 loss for box regression, β, δ_k and λ are weighting coefficients of UPL, CFL and CWA parts of the loss function. The parameter δ_k is proportional to the current iteration k and is set to gradually decrease weight of $\mathcal{L}_{IC}$ [12]. The parameter γ dictates the impact of the Wasserstein distance-based loss, $\mathcal{L}_{CWA}$ which is sensitive to its impact on the overall objective. A comprehensive depiction of the OD-CWA framework is presented in detail in Fig. 3.

6. Experimental Evaluation

6.1. Setup

Datasets This method utilises `PASCAL-VOC` [3] and `MS COCO` [17] dataset. First, we utilise `trainval` dataset of VOC for closed-set training, and then use a set of 20 VOC CLASSES and 60 non-VOC classes in COCO to evaluate the proposed method under myriad open-set conditions. Particularly, two different settings are considered, i.e., `VOC-COCO`-$\{\mathbf{T}_1, \mathbf{T}_2\}$ as per Han *et al*. [12]. We resort to similar dataset to maintain consistency. The open-set $\{\mathbf{T}_1\}$, contains $5k, 10k, 15k$ VOC testing images containing $\{20, 40, 60\}$ non-VOC classes and $\{\mathbf{T}_2\}$ was created with four combined datasets by increasing WI [8], each comprising $n = 5000$ VOC testing images and disjoint sets of $\{0.5n, n, 4n\}$ COCO images not overlapping with VOC classes. Now, we describe different metrics that are utilised for evaluation of our approach. **Wilderness Impact (WI) [8]** is used to measure the degree of unknown objects misclassified to known classes and has the following formulation, $\text{WI} = \left(\frac{P_{\mathcal{K}}}{P_{\mathcal{K} \cup \mathcal{U}}} - 1\right) \times 100$, where $P_{\mathcal{K}}$ and $P_{\mathcal{K} \cup \mathcal{U}}$ denote the precision of close-set and open-set classes and the metric WI is scaled by 100 for better presentation. When it comes to evaluation, the paper takes a very similar evaluation approach as per Han *et al*. [12]. **Absolute Open-Set Error (AOSE) [25]** is used, a metric used to count the number of misclassified unknown objects. Furthermore, we report the mean Average Precision (mAP) of known classes ($\text{mAP}_{\mathcal{K}}$). Lastly, we measure the novelty discovery ability by $AP_{\mathcal{U}}$ (AP of the unknown class). Note WI, AOSE, and $AP_{\mathcal{U}}$ are open-set metrics, and $\text{mAP}_{\mathcal{K}}$ is a close-set metric. **Implementation Details** In our methodology, we employ the architecture ResNet-50 [13] with a Feature Pyramid Network (FPN) [18] for all our methods. Some minor changes were made to the learning rate scheduler of Detectron2 [34] utilised inside the framework of OD [12]. A Stochastic Gradient Descent optimiser is used for training with an initial learning rate, momentum and weight decay to be 0.02, 0.9, and 10^{-4} respectively. Model training is carried out concurrently on 8 GPUs (**Tesla V100-SXM2-32GB**) with 16 images per batch. In regard to CFL, we follow the parameter settings used by OD.[4] For UPL, we follow the uncertainty guided hard example mining procedure and select top-3 sample examples for both foreground and background proposals. The hyperparameters α, β are set to, $1, 0.5$ respectively, δ_k is gradually decreased with every iteration k. For carrying out the optimal transportation, we utilise a package called as `Goemloss` [9] with tensorised PyTorch backend. The parameter p in the Sinkhorn distance loss corresponds to the power in the cost function. In our case, we choose $p = 1$, indicating the utilisation of the L_1 norm as the cost $d(x, y)$. The parameter blur $\nu = 0.1$ introduces a smoothing factor into the optimisation process to averts numerical instability, enhancing the overall stability of the Sinkhorn distance computation.

6.2. Main Results

The novelty of our paper lies in development of two main modelling approaches: Open-Det Class Wasserstein Anchor (OD-CWA) and Open-Det Spectral Normalisation (OD-SN) as per Eqs. 5 and 6, respectively. We compare these two approaches with 7 other methods, which also includes the current state-of-the-art method by [12], on VOC-COCO-$\{\mathbf{T}_1, \mathbf{T}_2\}$ dataset, which are exhibited in Tables 1

[4] All experiments are conducted using the exact training parameters outlined in Han et al. [12], except for our novel additions to the loss function, which ensures consistent comparison.

Method	VOC	VOC-COCO-20				VOC-COCO-40				VOC-COCO-60			
	$mAP_{K\uparrow}$	$WI_{\downarrow}$	$AOSE_{\downarrow}$	$mAP_{K\uparrow}$	$AP_{U\uparrow}$	$WI_{\downarrow}$	$AOSE_{\downarrow}$	$mAP_{K\uparrow}$	$AP_{U\uparrow}$	$WI_{\downarrow}$	$AOSE_{\downarrow}$	$mAP_{K\uparrow}$	$AP_{U\uparrow}$
FR-CNN [21]	**80.10**	18.39	15118	58.45	-	22.74	23391	55.26	-	18.49	25472	55.83	-
CAC [25]	79.70	19.99	16033	57.76	-	24.72	25274	55.04	-	20.21	27397	55.96	-
PROSER [38]	79.68	19.16	13035	57.66	10.92	24.15	19831	54.66	7.62	19.64	21322	55.20	3.25
ORE [14]	79.80	18.18	12811	58.25	2.60	22.40	19752	55.30	1.70	18.35	21415	55.47	0.53
DS [24]	80.04	16.98	12868	58.35	5.13	20.86	19775	55.31	3.39	17.22	21921	55.77	1.25
OD [12]	80.02	14.95	11286	**58.75**	14.93	18.23	16800	**55.83**	10.58	14.24	18250	**56.37**	4.36
OD-SN	79.66	12.96	9432	57.86	14.78	16.28	14118	55.36	10.54	12.76	15251	56.07	4.17
OD-CWA	79.20	**11.70**	**8748**	57.58	**15.36**	**14.58**	**13037**	55.26	**10.98**	**11.55**	**14984**	55.73	**4.45**

Table 1. Comparison of OD-SN and OD-CWA (trained on ResNet-50 backbone) with other methods on VOC and VOC-COCO-$\{\mathbf{T}_1\}$. The close-set performance ($mAP_{\mathcal{K}}$) on VOC, and both close-set ($mAP_{\mathcal{K}}$) and open-set ($WI, AOSE, AP_{\mathcal{U}}$) performance of different methods on VOC-COCO-20, 40, 60 are reported. Numbers in bold black colour indicates best performing on that metric, and bold orange indicates second best. Significant improvements in $WI, AOSE$ and $AP_{\mathcal{U}}$ are achieved at the expense of a slight decrease in $mAP_{\mathcal{K}}$.

Method	VOC-COCO-0.5n				VOC-COCO-n				VOC-COCO-4n			
	$WI_{\downarrow}$	$AOSE_{\downarrow}$	$mAP_{K\uparrow}$	$AP_{U\uparrow}$	$WI_{\downarrow}$	$AOSE_{\downarrow}$	$mAP_{K\uparrow}$	$AP_{U\uparrow}$	$WI_{\downarrow}$	$AOSE_{\downarrow}$	$mAP_{K\uparrow}$	$AP_{U\uparrow}$
FR-CNN [21]	9.25	6015	77.97	-	16.14	12409	74.52	-	32.89	48618	63.92	-
CAC [25]	9.92	6332	77.90	-	16.93	13114	74.40	-	35.42	52425	63.99	-
PROSER [38]	9.32	5105	77.35	7.48	16.65	10601	73.55	8.88	34.60	41569	63.09	11.15
ORE [14]	8.39	4945	77.84	1.75	15.36	10568	74.34	1.81	32.40	40865	64.59	2.14
DS [24]	8.30	4862	77.78	2.89	15.43	10136	73.67	4.11	31.79	39388	63.12	5.64
OD [12]	6.44	3944	**78.61**	**9.05**	11.70	8282	**75.56**	**12.30**	26.69	32419	**65.55**	16.76
OD-SN	6.01	3084	78.16	8.24	11.30	6439	75.11	11.92	26.50	26261	64.49	16.48
OD-CWA	**5.21**	**2780**	78.30	8.30	**9.95**	**6001**	75.10	12.26	**23.31**	**24072**	64.75	**17.11**

Table 2. Comparison of OD-SN and OD-CWA (trained on ResNet-50 backbone) with other methods on VOC and VOC-COCO-$\mathbf{T}_2$. Numbers in bold black colour indicates improvement of that metric, and bold orange indicates deterioration of that metric. Numbers in bold black colour indicates best performing on that metric, and bold orange indicates second best.

Method	δ_k	λ	VOC	VOC-COCO-20			
			$mAP_{K\uparrow}$	$WI_{\downarrow}$	$AOSE_{\downarrow}$	$mAP_{K\uparrow}$	$AP_{U\uparrow}$
OD [12]	0.1	-	83.29	12.51	9875	63.17	15.77
OD-SN	0.1	-	82.49	14.39	**7306**	61.59	16.45
OD-CWA	0.25	1.3	**83.64**	12.44	7880	63.18	14.06
OD-CWA	0.18	1.3	83.06	**10.32**	8888	62.93	15.34
OD-CWA	0.21	1.6	79.20	12.16	10007	57.09	15.53
OD-CWA	0.21	1.83	83.15	10.44	8951	63.20	15.41
OD-CWA	0.21	1.7	83.34	10.35	8946	**63.59**	**18.22**

Table 3. Comparison of the Swin-Transformer [22] backbone-based proposed method with Object Detection (OD) on VOC and VOC-COCO-$\mathbf{T}_1$, examining the impacts of varying δ_k and λ on different metrics. Parameter λ is in the order of 10^{-3}. OD-CWA (last row) outperforms OD in every aspect significantly.

and 2. When we train a model as per Eq. 5 and evaluate for VOC and VOC-COCO-20 classes in $\mathbf{T}_1$, we can see that there is a decrease of 12% & 16.4% for metrics WI and AOSE, respectively, while there is a 1% reduction in mAP$_{\mathcal{K}}$ and $AP_{\mathcal{U}}$ for the ResNet-50 backbone. Similar effects can be observed in VOC-COCO-$\{40, 60\}$ in $\mathbf{T}_1$. On almost all metrics for $\mathbf{T}_2$ dataset, similar effects of substantial improvement in WI and AOSE with slight deterioration in mAP$_{\mathcal{K}}$ and $AP_{\mathcal{U}}$ is observed for the ResNet-50 backbone. Further, we have added Class Anchor Clustering (CAC) to the Table 1 and 2, and it suffers from poor performance just by itself. The second approach, OD-CWA, utilises SN along with the addition of $\mathcal{L}_{CWA}$, $\mathcal{L}_{IC}$ and $\mathcal{L}_{UP}$ as per Eq. 5. As a result of this combination on the ResNet-50 backbone, the improvement in open-set performance is significant, i.e., improvement of $18\%, 22\%$ and 2.8% on open-set metrics WI, AOSE and AP$_{\mathcal{U}}$, respectively. The improvement can be best captured in Fig. 5 which depicts qualitative results comparing approaches OD-CWA and OD. Further, when we use OD-CWA approach to train a detector based on a Swin-T backbone, we can see that our detector surpasses OD by a substantial amount on all the metrics, e.g., Table 3 suggests there is an improvement of $\approx 21\%, 9.4\%, 0.6\%$ and 15.5% on all 4 metrics. We conduct some ablation studies in Table 4 to see how individual components, i.e., SN, CFL, UPL and CWA contribute towards the performance. Adding SN to the method OD improved WI, AOSE by 13.3% and 16.4%, respectively, and deteriorated the $AP_{\mathcal{U}}$

δ_k	λ	$WI_{\downarrow}$	$AOSE_{\downarrow}$	$mAP_{K\uparrow}$	$AP_{U\uparrow}$
0.35	-	12.96	9432	**57.86**	14.78
0.1	1.3	19.07	7899	54.94	14.38
0.35	2.6	10.46	9803	56.19	15.03
0.35	4.6	**10.40**	9566	56.64	14.54
0.29	4.6	11.52	9312	57.02	14.18
0.26	4.6	11.20	9473	57.02	14.19
0.21	1.7	11.70	**8748**	**57.86**	**15.36**

Table 4. Effects of δ_k and λ in the combined loss function for model trained using ResNet-50 backbone and evaluated on VOC-COCO-20 dataset. Parameter λ is in the order of 10^{-3}. The first row represents OD and the last row shows the method OD-CWA.

slightly from OD. Extra analysis of how parameters δ and λ affects the performance of the detector on both ResNet-50 and Swin-T backbone is shown in Table 5 and 3. Results pertaining to blur parameter ν that governs the smoothing/regularisation of Sinkhorn divergences (as per eq 3) can be found in Table-7. We select $\nu = 1$ based purely on empirical grounds, aiming for optimal performance on all metrics. We conduct some ablation studies to throw light

SN	CFL	CWA	UPL	$WI_{\downarrow}$	$AOSE_{\downarrow}$	$mAP_{K\uparrow}$	$AP_{U\uparrow}$
-	✓	-	-	17.92	15162	58.54	-
-	-	-	✓	16.47	12018	57.91	14.27
	✓		✓	14.95	11286	**58.75**	14.93
-	✓	✓	✓	12.42	10193	57.60	15.09
✓	✓		✓	12.96	9432	57.86	14.78
✓	✓	✓	✓	**11.70**	**8748**	**57.58**	**15.36**

Table 5. Ablation study of individual components for VOC-COCO-20 open-set data obtained for R-50 backbone. The third row shows method OD and the last row shows OD-CWA.

CFL	CWA	UPL	$\frac{\Sigma}{\mu}_{\downarrow}$	DI$_{\uparrow}$	CHI$_{\uparrow}$	HI$_{\uparrow}$	DBI$_{\downarrow}$	XBI$_{\downarrow}$
✓	-	✓	0.824	0.025	449.3	0.91	6.52	0.59
✓	✓	✓	0.04	0.01	629.27	0.89	4.24	0.05

Table 6. Quantitative analyses of intra-cluster and inter-clusters variances and distances calculated using different metrics corresponding to CFL, UPL and CWA on closed-set, i.e., VOC-20 classes for model trained on R-50 backbone.

on how each part of the combined loss function Eq. (5) behaves, taking into account the compactness of the clusters and how separated are the classes (closed-set) from each other. The results[5] can be seen from the Table 6. Intra-class variances (Σ) are the variances of Euclidean distances obtained between the proposal embeddings of detections and

[5]The intra-class and inter-class evaluation results presented here diverge from those in the study by Han et al. [12]. This disparity stems from the absence of codes necessary to reproduce their results.

ν	VOC	VOC-COCO-20			
	$mAP_{K\uparrow}$	$WI_{\downarrow}$	$AOSE_{\downarrow}$	$mAP_{K\uparrow}$	$AP_{U\uparrow}$
0.5	**79.26**	12.29	9530	57.07	13.39
0.3	79.11	11.78	9175	57.31	14.51
0.2	78.83	12.17	9178	57.44	**16.03**
0.15	79.23	12.23	9361	57.46	14.54
0.1	79.20	**11.70**	**8748**	**57.58**	15.36

Table 7. Effects of variation of blur ν in the combined loss function for model trained using ResNet-50 backbone and evaluated on VOC-COCO-20 dataset. The blur is a regularisation parameter that governs evaluation of Sinkhorn divergence [1].

the centroid of a particular class. Inter-class distance (μ) average of Euclidean distance between all the class centres of different classes. The ratio of $\frac{\Sigma}{\mu} = \frac{\text{Var}(\mathbb{E}_j(\mathbf{z}_{j,d} - \mathbb{E}_d(\mathbf{z}_{j,d})))}{\sum_{j,k\in\{1,C\},j\neq k} \|\mathbf{z}_i - \mathbf{z}_j\|_2}$ is reported in Table-6. Along with this ratio, we also add a couple of other widely used indices, e.g., Dunn Index (DI), Calinski-Harabasz Index (CHI), Hubert Index (HI), Davies Bouldin index (DBI) and Xie-Beni Index (XBI). The details of these indices can be found in [7]. It is important to recognise that there isn't a single optimal metric for evaluating intra-cluster and inter-cluster properties, so we have chosen a few popular ones. When, CWA is added to CFL and UPL, there is a slight drop in performance for two out of the six indices, and good improvement in the rest indices.

7. Conclusion

A novel open-set detector, OD-CWA specifically designed to address the challenge of open-set detection is presented. OD-CWA aims to enhance the discrimination of low-density latent regions and improve clustering through the integration of three key components: IC loss, CWA loss, and UP loss. Both CWA and IC components are guided by spectral normalisation of weights in the final output layer. These two losses along with UP loss further enhances the model's capability in flagging unknown objects in the test instances. The promising empirical results and a couple of novel additions suggest that this approach has the potential to pave the way for new research directions in OSOD.

Limitations: We notice that this approach still suffers from reasonable open-set errors, especially when there are a lot of objects in the image. Sometimes, there are instances where the detector is confused during inference on an unknown class image and its predictions are both unknown with high score and known with medium prediction score. We aim to redirect our attention towards rediscovering $\mathcal{L}_{UP}$ in light of this observed confusion. Furthermore, as Wasserstein distance approach is new and comes with some promising theoretical results, our future work will predominantly centre on harnessing these guarantees to derive generalisation bounds for open-set conditions.

References

[1] The sinkhorn-knopp algorithm: Convergence and applications. *SIAM Journal on Matrix Analysis and Applications*, 30(1):261–15, 2008. Copyright - Copyright] © 2008 Society for Industrial and Applied Mathematics; Last updated - 2022-10-20. 4, 8

[2] Martin Arjovsky, Soumith Chintala, and Léon Bottou. Wasserstein generative adversarial networks. In *Proceedings of the 34th International Conference on Machine Learning*, pages 214–223. PMLR, 2017. 4

[3] P. Bentley, G. Nordehn, M. Coimbra, and S. Mannor. The PASCAL Classifying Heart Sounds Challenge 2011 (CHSC2011) Results. http://www.peterjbentley.com/heartchallenge/index.html. 6

[4] Patrick Billingsley. *Probability and measure*. John Wiley & Sons, 2008. 4

[5] Olivier Chapelle, Bernhard Schölkopf, and Alexander Zien, editors. *Semi-Supervised Learning*. The MIT Press, 2006. 1

[6] Nicolas Courty, Rémi Flamary, and Devis Tuia. Domain adaptation with regularized optimal transport. In *Machine Learning and Knowledge Discovery in Databases: European Conference, ECML PKDD 2014, Nancy, France, September 15-19, 2014. Proceedings, Part I 14*, pages 274–289. Springer, 2014. 1, 2, 4

[7] Bernard Desgraupes. Clustering indices. 2016. 8

[8] Akshay Raj Dhamija, Manuel Günther, Jonathan Ventura, and Terrance E. Boult. The overlooked elephant of object detection: Open set. *2020 IEEE Winter Conference on Applications of Computer Vision (WACV)*, pages 1010–1019, 2020. 6

[9] Jean Feydy, Thibault Séjourné, François-Xavier Vialard, Shun-ichi Amari, Alain Trouve, and Gabriel Peyré. Interpolating between optimal transport and mmd using sinkhorn divergences. In *The 22nd International Conference on Artificial Intelligence and Statistics*, pages 2681–2690, 2019. 6

[10] Yarin Gal and Zoubin Ghahramani. Dropout as a bayesian approximation: Representing model uncertainty in deep learning. In *Proceedings of The 33rd International Conference on Machine Learning*, pages 1050–1059, New York, New York, USA, 2016. PMLR. 2

[11] Yves Grandvalet and Yoshua Bengio. Semi-supervised learning by entropy minimization. In *Advances in Neural Information Processing Systems*. MIT Press, 2004. 1

[12] Jiaming Han, Yuqiang Ren, Jian Ding, Xingjia Pan, Ke Yan, and Gui-Song Xia. Expanding low-density latent regions for open-set object detection. In *Proceedings of the IEEE/CVF Conference on Computer Vision and Pattern Recognition (CVPR)*, 2022. 1, 2, 3, 4, 5, 6, 7, 8

[13] Kaiming He, Xiangyu Zhang, Shaoqing Ren, and Jian Sun. Deep residual learning for image recognition. In *2016 IEEE Conference on Computer Vision and Pattern Recognition (CVPR)*, pages 770–778, 2016. 6

[14] K J Joseph, Salman Khan, Fahad Shahbaz Khan, and Vineeth N Balasubramanian. Towards open world object detection. In *Proceedings of the IEEE/CVF Conference on Computer Vision and Pattern Recognition (CVPR 2021)*, 2021. 1, 2, 3, 7

[15] Prannay Khosla, Piotr Teterwak, Chen Wang, Aaron Sarna, Yonglong Tian, Phillip Isola, Aaron Maschinot, Ce Liu, and Dilip Krishnan. Supervised contrastive learning. *Advances in neural information processing systems*, 33:18661–18673, 2020. 5

[16] Balaji Lakshminarayanan, Alexander Pritzel, and Charles Blundell. Simple and scalable predictive uncertainty estimation using deep ensembles, 2017. 2

[17] Tsung-Yi Lin, Michael Maire, Serge Belongie, James Hays, Pietro Perona, Deva Ramanan, Piotr Dollár, and C. Lawrence Zitnick. Microsoft coco: Common objects in context. In *Computer Vision – ECCV 2014*, pages 740–755, Cham, 2014. Springer International Publishing. 6

[18] Tsung-Yi Lin, Piotr Dollár, Ross B. Girshick, Kaiming He, Bharath Hariharan, and Serge J. Belongie. Feature pyramid networks for object detection. In *CVPR*, pages 936–944. IEEE Computer Society, 2017. 6

[19] Jeremiah Liu, Zi Lin, Shreyas Padhy, Dustin Tran, Tania Bedrax Weiss, and Balaji Lakshminarayanan. Simple and principled uncertainty estimation with deterministic deep learning via distance awareness. In *Advances in Neural Information Processing Systems*, pages 7498–7512. Curran Associates, Inc., 2020. 1, 5

[20] Shilong Liu, Zhaoyang Zeng, Tianhe Ren, Feng Li, Hao Zhang, Jie Yang, Chunyuan Li, Jianwei Yang, Hang Su, Jun Zhu, and Lei Zhang. Grounding dino: Marrying dino with grounded pre-training for open-set object detection, 2023. 2

[21] Ziwei Liu, Zhongqi Miao, Xiaohang Zhan, Jiayun Wang, Boqing Gong, and Stella X. Yu. Large-scale long-tailed recognition in an open world. In *IEEE Conference on Computer Vision and Pattern Recognition (CVPR)*, 2019. 7

[22] Ze Liu, Yutong Lin, Yue Cao, Han Hu, Yixuan Wei, Zheng Zhang, Stephen Lin, and Baining Guo. Swin transformer: Hierarchical vision transformer using shifted windows. In *Proceedings of the IEEE/CVF international conference on computer vision*, pages 10012–10022, 2021. 7

[23] Leland McInnes, John Healy, and James Melville. Umap: Uniform manifold approximation and projection for dimension reduction, 2020. 2, 1

[24] Dimity Miller, Lachlan Nicholson, Feras Dayoub, and Niko Sünderhauf. Dropout sampling for robust object detection in open-set conditions. In *2018 IEEE International Conference on Robotics and Automation (ICRA)*, pages 3243–3249. IEEE, 2018. 1, 2, 7

[25] Dimity Miller, Niko Sünderhauf, Michael Milford, and Feras Dayoub. Uncertainty for identifying open-set errors in visual object detection. *IEEE Robotics and Automation Letters*, 7 (1):215–222, 2021. 1, 2, 6, 7

[26] Dimity Miller, Niko Sunderhauf, Michael Milford, and Feras Dayoub. Class anchor clustering: A loss for distance-based open set recognition. In *Proceedings of the IEEE/CVF Winter Conference on Applications of Computer Vision*, pages 3570–3578, 2021. 4, 5

[27] Aaditya Ramdas, Nicolás García Trillos, and Marco Cuturi. On wasserstein two-sample testing and related families of nonparametric tests. *Entropy*, 19(2):47, 2017. 4

[28] Shaoqing Ren, Kaiming He, Ross Girshick, and Jian Sun. Faster r-cnn: Towards real-time object detection with region proposal networks. *Advances in neural information processing systems*, 28, 2015. 4

[29] Walter J. Scheirer, Anderson de Rezende Rocha, Archana Sapkota, and Terrance E. Boult. Toward open set recognition. *IEEE Transactions on Pattern Analysis and Machine Intelligence*, 35(7):1757–1772, 2013. 1, 2

[30] Walter J. Scheirer, Lalit Prithwiraj Jain, and Terrance E. Boult. Probability models for open set recognition. *IEEE Transactions on Pattern Analysis and Machine Intelligence*, 36(11):2317–2324, 2014. 2

[31] Jian Shen, Yanru Qu, Weinan Zhang, and Yong Yu. Wasserstein distance guided representation learning for domain adaptation. In *Proceedings of the AAAI Conference on Artificial Intelligence*, 2018. 2, 4

[32] Cédric Villani. *Optimal transport – Old and new*, pages xxii+973. 2008. 4

[33] Yandong Wen, Kaipeng Zhang, Zhifeng Li, and Yu Qiao. A discriminative feature learning approach for deep face recognition. In *Computer Vision–ECCV 2016: 14th European Conference, Amsterdam, The Netherlands, October 11–14, 2016, Proceedings, Part VII 14*, pages 499–515. Springer, 2016. 5

[34] Yuxin Wu, Alexander Kirillov, Francisco Massa, Wan-Yen Lo, and Ross Girshick. Detectron2. https://github.com/facebookresearch/detectron2, 2019. 6

[35] Alireza Zareian, Kevin Dela Rosa, Derek Hao Hu, and Shih-Fu Chang. Open-vocabulary object detection using captions. In *Proceedings of the IEEE/CVF Conference on Computer Vision and Pattern Recognition*, pages 14393–14402, 2021. 3

[36] Hao Zhang, Feng Li, Shilong Liu, Lei Zhang, Hang Su, Jun Zhu, Lionel M Ni, and Heung-Yeung Shum. Dino: Detr with improved denoising anchor boxes for end-to-end object detection. *arXiv preprint arXiv:2203.03605*, 2022. 3

[37] Jiyang Zheng, Weihao Li, Jie Hong, Lars Petersson, and Nick Barnes. Towards open-set object detection and discovery. In *Proceedings of the IEEE/CVF Conference on Computer Vision and Pattern Recognition*, pages 3961–3970, 2022. 3

[38] Da-Wei Zhou, Han-Jia Ye, and De-Chuan Zhan. Learning placeholders for open-set recognition. In *CVPR*, pages 4401–4410, 2021. 7

Wasserstein Distance-based Expansion of Low-Density Latent Regions for Unknown Class Detection

Supplementary Material

A. Visualisation of proposal embeddings

Figure-B1 provides a U-MAP [23]-based visual representation of proposal embeddings for closed-set ($C_{\mathcal{K}}$) class detections. The top two subplots demonstrate the reduced-dimensional proposal embeddings of detections for baseline (OD) and OD-CWA approaches. OD-CWA exhibits more cohesive clusters compared to OD. In the bottom two subplots, we narrow our focus to a subset of detections from the top plots and overlay unknown detections (depicted by black × symbols) to emphasise the dispersion of unknowns amid known objects. This shows the scattering of low-density latent regions. The plots are appropriately rotated for improved visibility.

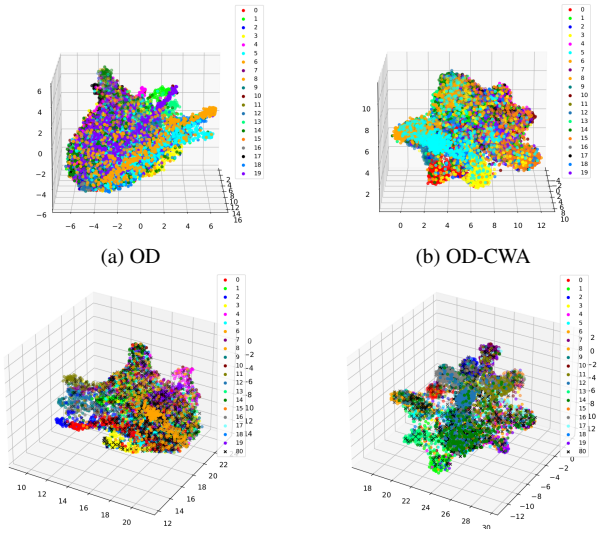

(a) OD (b) OD-CWA

(c) OD (d) OD-CWA

Figure B1. A full U-MAP [23] visualisation of proposal embeddings $\mathbf{F}_d \in \mathbb{R}^{128}$, d refers to number of detections, for VOC-20 closed-set classes. Top two subplots shows all detections of known objects and bottom two subplots shows subset of known along with unknown embeddings to show scattering of low-density regions.

B. Additional Experimental Information

This section provides some comprehensive results, i.e.,

1. elaboration on additional experimental details that were omitted in the main paper due to space limitations. This includes the presentation of two tables (Table B1 and B2) related to performance of Swin-T backbone (part of which was in the main paper). Table B3 summarises performance of OD and OD-CWA based on two different backbones on VOCO-COCO-20.
2. training time aspects of two distinct approaches, namely OD and OD-CWA can be found in Fig-B3. Each approach is examined under two different backbones.
3. Inclusion of pertinent details for reproducing the codes developed by Han et al. [12]. This section serves as a valuable resource for researchers seeking to replicate and validate the outcomes of our study, fostering transparency and reproducibility in scientific endeavours.

B.1. Experimental Setup Details

The experimental setup used for training and evaluation is outlined in this section. To optimise the utilisation of high-performance computing resources, we conducted our experiments on `NVIDIA DGX` clusters integrated with Kubernetes. The `NVIDIA DGX` systems, featuring `Tesla V100-SXM2-32`GB GPUs, formed our computing infrastructure. The combination of PyTorch, Kubernetes, and NVIDIA DGX contributed to the efficiency of our experiments, enabling expedited training and evaluation of models within a distributed computing environment.

Figure B2. Failure Cases for OD-CWA. It does not imply the success by OD, rather it means there were misclassifications and confusion arising from cluttered images.

B.2. Comments on utilising codes by Han *et al.* [12]

All qualitative results presented herein, as well as those detailed in the main paper, were derived through the training of a model utilising the $\mathcal{L}_{\text{OD-CWA}}$ for $80,000$ iterations. The inference phase, performed to facilitate the comparison of results on a set of images, is depicted in Fig-B4. The model training employed precise parameters consistent with the OD framework [12]. However, attempting to execute OD by replicating the provided codes from the GitHub repos-

δ_k	λ	VOC	VOC-COCO-20				VOC-COCO-40				VOC-COCO-60			
		$mAP_{K\uparrow}$	$WI_{\downarrow}$	$AOSE_{\downarrow}$	$mAP_{K\uparrow}$	$AP_{U\uparrow}$	$WI_{\downarrow}$	$AOSE_{\downarrow}$	$mAP_{K\uparrow}$	$AP_{U\uparrow}$	$WI_{\downarrow}$	$AOSE_{\downarrow}$	$mAP_{K\uparrow}$	$AP_{U\uparrow}$
0.25	1.3	**83.61**	10.57	9038	63.46	13.86	12.78	12880	61.18	9.96	9.73	13079	62.08	3.47
0.18	1.3	83.06	**10.32**	8888	62.93	15.34	12.91	12700	60.57	10.73	9.91	13226	61.58	3.82
0.21	1.6	79.20	12.16	10007	57.09	15.53	**12.44**	12792	61.24	10.80	**9.61**	13178	62.02	3.79
0.21	1.83	83.15	10.44	8951	63.20	15.41	12.55	**12667**	60.70	10.59	9.71	13065	61.60	3.79
0.21	1.7	83.34	10.35	**8946**	**63.59**	**18.22**	12.73	12710	**61.26**	**12.02**	9.76	**12998**	**62.23**	**4.28**

Table B1. Additional results of Swin-T backbone-based proposed method OD-CWA evaluated on VOC and VOC-COCO-$\{\mathbf{T}_1\}$. This was skipped in the main paper because of space constraints, however, the first 4 columns were shown in the main paper.

δ_k	λ	VOC-COCO-0.5n				VOC-COCO-n				VOC-COCO-2n				VOC-COCO-4n			
		$WI_{\downarrow}$	$AOSE_{\downarrow}$	$mAP_{K\uparrow}$	$AP_{U\uparrow}$	$WI_{\downarrow}$	$AOSE_{\downarrow}$	$mAP_{K\uparrow}$	$AP_{U\uparrow}$	$WI_{\downarrow}$	$AOSE_{\downarrow}$	$mAP_{K\uparrow}$	$AP_{U\uparrow}$	$WI_{\downarrow}$	$AOSE_{\downarrow}$	$mAP_{K\uparrow}$	$AP_{U\uparrow}$
0.25	1.3	3.98	2425	83.56	6.93	7.96	5303	**80.62**	10.23	14.22	10666	**76.28**	13.17	21.80	21390	70.27	15.37
0.18	1.3	3.98	2538	82.90	7.70	8.02	5252	79.89	11.11	14.19	10672	75.61	13.85	22.07	21451	69.59	15.96
0.21	1.6	4.02	2427	83.33	7.59	7.82	5210	80.25	10.75	13.91	10673	76.00	13.75	21.68	21286	70.07	16.02
0.21	1.83	4.26	2377	82.91	8.11	8.21	**5079**	79.91	11.22	14.44	**10464**	75.73	13.85	22.55	**20764**	70.16	15.81
0.21	1.7	**3.73**	**2429**	**83.24**	**9.45**	**7.36**	5162	80.25	**12.67**	**13.14**	10576	76.08	**15.01**	**20.64**	21255	**70.55**	**16.87**

Table B2. Additional results of Swin-T backbone-based proposed method OD-CWA evaluated on VOC and VOC-COCO-$\mathbf{T}_2$ i.e., disjoint sets $\{0.5n, n, 2n, 4n\}$. These results were skipped in the main paper because of space constraints. VOC-COCO-$2n$ is not a separate dataset, rather a part of VOC-COCO-$\{\mathbf{T}_2\}$ [12].

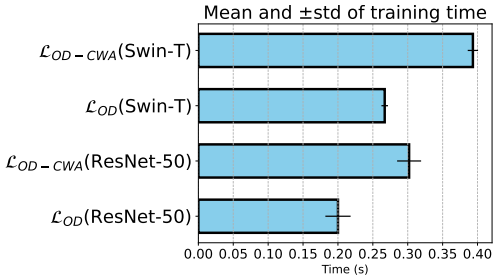

Figure B3. Training time for models trained with loss functions, $\mathcal{L}_{OD}$ and $\mathcal{L}_{OD-CWA}$ taking into account two different backbones, i.e., ResNet-50 and Swin-T. The training time stamps are collected in seconds and measured per 20 iterations ran on 8 gpus.

itory authored by Han et al. [12] revealed issues, necessitating modifications for successful run. Challenges such as version mismatches resulted in extended errors. To address this in future, we will be releasing codes (upon acceptance) which leverages docker for model training, ensuring a seamless and error-free execution environment that alleviates version discrepancies, guaranteeing a consistent experimental setup.

B.3. Comprehensive Qualitative Comparison

Fig-B4 provides a detailed qualitative analysis comparing the baseline method OD with our developed approach OD-CWA. OD excels in detecting unknowns, evident in figure pairs $2, 3, 4, 5, 6, 7, 12, 13, 15, 17, 21$. However, OD-CWA surpasses these capabilities by not only enhancing the prediction scores of unknowns but also reducing confusion. For instance, in figure pair 7, OD detects one zebra as a known object (person) and the other as unknown with a predictive score of 88%. In contrast, OD-CWA confidently predicts both zebras as unknown with much higher predictive power. Similar improvements are observed in other instances, such as figure pairs $12, 13, 15$, and more.

Method	Backbone	$WI_{\downarrow}$	$AOSE_{\downarrow}$	$mAP_{K\uparrow}$	$AP_{U\uparrow}$
OD	ResNet-50	14.95	11286	**58.75**	14.93
	Swin-T	12.51	9875	63.17	15.77
OD-CWA	ResNet-50	**11.70**	**8748**	57.58	**15.36**
	Swin-T	**10.35**	**8946**	**63.59**	**18.22**

Table B3. Summary of OD and OD-CWA results on ResNet-50 and Swin-T backbones. Bold represents the best of two methods

B.4. Failure Cases

Fig-B2 showcases instances considered as failures when tested by our method OD-CWA. Six image examples are provided. In the first image, OD-CWA identifies the statue as unknown but fails to recognise distinctive objects such as traffic lights. In other cases, such as the 2^{nd} image, the detector identifies an aeroplane but is confused by the flight engines, mistaking them for an unknown object. Similarly, in the 4^{th} instance, the detector categorises traffic lights as unknown, but a part of the lights is identified as a chair. It's important to note that even though these instances are considered failures, it doesn't imply correct identification by the baseline (OD); in fact, the baseline inference results were worse for these cases.

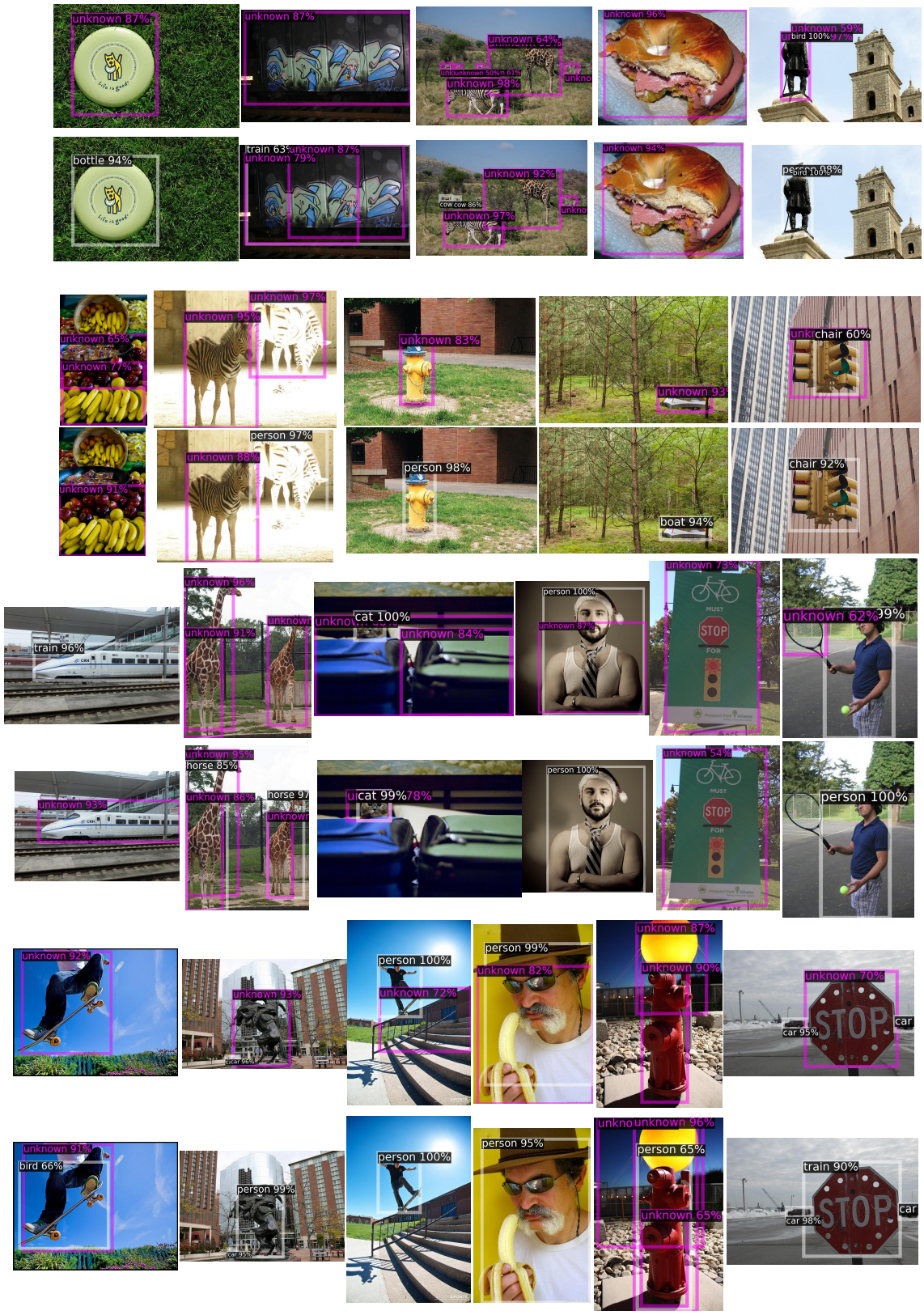

Figure B4. Qualitative comparisons between OD and proposed OD-CWA. In each pair of images, the top image represents OD-CWA, while the other corresponds to OD. Objects marked in purple indicate unknown entities, while white denotes known objects. For instance, in the first image pair, the object labelled as a Frisbee (unknown) is misclassified as a bottle by the model trained with OD [12]. In contrast, OD-CWA correctly identifies the object as belonging to an unknown class.